Asian Journal of Chemistry; 38, No. 6 (2026), 1411-1422
ASIAN JOURNAL OF CHEMISTRY
https://doi.org/10.14233/ajchem.2026.35725

Synergistic Effects of Silver Incorporation on the Electrochemical Behaviour of $NiMoO_4$ Nanostructures

S. VIJIPRIYA[1], M. ANUJENCY[1], N.P. PRATHEEB[2] and M. MOHAMED IBRAHIM[1,*]

[1]PG and Research and Department of Physics, Kongunadu Arts and Science College, Coimbatore-641029, India
[2]Department of Physical Science, Nova College of Education, Coimbatore-641047, India

*Corresponding author: E-mail: mibrahim27@gmail.com

Received: 8 February 2026 *Accepted*: 11 April 2026 *Published online*: 31 May 2026 AJC-22367

Electrode materials for electrochemical energy storage require high capacitance, rapid charge–discharge capability and excellent cycling stability. In present study, the pure and Ag-incorporated $NiMoO_4$ nanostructures containing 3, 5 and 7 wt.% Ag were synthesised *via* a simple co-precipitation method and systematically investigated. X-ray diffraction confirmed the formation of phase-pure monoclinic $NiMoO_4$ without secondary Ag phases, indicating successful Ag incorporation. SEM analysis showed improved particle dispersion and enhanced porosity, contributing to higher electrochemically active surface area and improved charge transport. Raman and XPS studies revealed Ag-induced lattice distortion and oxygen-vacancy-rich defect sites, which facilitate electron transfer and redox activity. The Ag (7 wt.%)-$NiMoO_4$ electrode exhibited enhanced electrochemical performance, delivering specific capacitances of 642.12 F g^{-1} (CV) and 1066.12 F g^{-1} (GCD), along with excellent cycling stability of 97.81% capacitance retention after 5000 cycles. The enhanced conductivity, defect-mediated charge transport and optimised ion diffusion synergistically contribute to improve the performance.

Keywords: $NiMoO_4$, Silver, Supercapacitor, Defect engineering, Oxygen vacancies.

INTRODUCTION

Supercapacitor systems have attracted significant attention as advanced energy-storage devices due to their high-power density, rapid charge-discharge capability and long cycle life. The performance of supercapacitors is primarily governed by the properties of the electrode material, particularly its electrochemically active surface area, electrical conductivity and ion transport characteristics [1]. Pseudocapacitive transition-metal compounds are of particular interest as aqueous supercapacitors since Faradaic redox reactions can allow much higher charge storage than carbon based purely electrostatic electrodes [1].

Nickel molybdate ($NiMoO_4$) is one such promising pseudocapacitive material with a rich redox chemistry and structural flexibility of their various polymorphs, having different environmental coordination atoms and electronic characteristics [2]. Various $NiMoO_4$ nanoarchitectures such as nanowires, nanosheets, hierarchical flowers and core-shell arrays have been demonstrated to be of high capacitance and high cycling stability due to maximisation of electrolyte contact and minimisation ion/electron diffusion pathways [3-7]. Despite all these benefits, pure $NiMoO_4$ inherently exhibits low electrical conductivity and low ionic transportation, constraining the number of redox-active sites, particularly in high charge-discharge rates [8,9]. Therefore, it is crucial to enhance conductivity and interfacial transport to enhance electrochemical activity of $NiMoO_4$ based electrodes.

It has already been demonstrated that the optimisation of conductive pathways, defect chemistry (especially oxygen vacancies) and hierarchical porosity in a synergistic manner can considerably lower the charge-transfer kinetics and enhance the density of electrochemically accessible Faradaic sites [10]. $NiMoO_4$ Electrodes containing oxygen vacancies or oxygen deficient/carbon-coated surfaces exhibit enhanced electrical conductivity, improved redox activity and superior cycling stability. The formation of these defect sites is consistently confirmed through complementary structural and spectroscopic techniques including X-ray diffraction (XRD), Raman spectroscopy and X-ray photoelectron spectroscopy (XPS) [8]. Moreover, multicomponent approaches, such as coupling $NiMoO_4$ with reduced graphene oxide or building heterostructured and

core shell structures, also show that interfacial charge transfer and mesoporosity are important in achieving high performance rates [11,12]. In this context, incorporation of silver (Ag) offers a good avenue of enhancing electronic transport and defect state modulation in transition-metal oxides. It has been shown that Ag incorporation significantly improves the pseudocapacitive behaviour by enhancing conductivity and enhancing the kinetics of charge-transfer [13]. In addition, lattice perturbation caused by Ag, usually expressed through the displacement and broadening of Raman peaks, are the signs of local distortion and breaking of symmetry within the oxide frameworks [14]. Silver was also demonstrated to facilitate the formation of defects and enhance the electrochemically active surface area resulting in the enhancement of charge storage capacity of different Ag-modified oxide systems [15,16]. The results indicate that Ag incorporation in $NiMoO_4$ may be able to improve the electronic conductivity, defect density and ion diffusion to generate a synergistic effect on the electrochemical performance.

Although Ag-modified $NiMoO_4$ systems have been previously investigated, most reported studies are based on hydrothermal, microwave-assisted or composite-assisted synthesis approaches. In this work, Ag incorporation (3-7 wt.%) into $NiMoO_4$ is achieved through a simple co-precipitation approach followed by controlled thermal treatment, which provides a scalable and cost-effective route for tailoring electrochemical properties. The present study systematically correlates Ag concentration with structural evolution, defect chemistry and electrochemical behaviour using complementary characterisation techniques (XRD, SEM-EDS, XPS and electrochemical analysis). This work therefore provides new insight into how controlled Ag incorporation modifies conductivity, ion transport pathways and pseudocapacitive performance in $NiMoO_4$ electrodes.

EXPERIMENTAL

Analytical grade silver nitrate ($AgNO_3$), ammonium molybdate tetrahydrate ($(NH_4)_6Mo_7O_{24}\cdot 4H_2O$), nickel nitrate hexahydrate ($Ni(NO_3)_2\cdot 6H_2O$), NaOH pellets, ethanol and deionised water were used.

Preparation of pristine $NiMoO_4$ and Ag doped $NiMoO_4$ by coprecipitation method: $NiMoO_4$ nanoparticles were prepared in a simple co-precipitation process where ammonium heptamolybdate tetrahydrate and nickel nitrate hexahydrate were dissolved in deionised water separately then mixed under stirring followed by controlled drop by drop titration of the two solutions with 0.1 M NaOH to produce a precursor of green nickel-molybdate hydroxide which was then allowed to age (1 h) to complete the precipitation process. To obtain the precipitate, centrifugation was used to isolate the material, followed by thermal treatment in air at 750 ºC over 5 h to attain phase transformation and a higher degree of crystallinity, which in turn can be used to control the stability and electrochemical characteristics of the $NiMoO_4$ nanostructure under operating conditions. It is predicted to prefer thermodynamically stable α-$NiMoO_4$ polymorph over β-$NiMoO_4$ at the expense of phase energetics and sensitivity of $NiMoO_4$ to thermal-history effects, although heating ramps may affect nanoarchitectures. The same procedure was repeated to produce samples Ag-doped, except that silver nitrate was co-dissolved with nickel nitrate so that the ratio of Ag to the final oxide was 3, 5 and 7 wt.% and then the same procedure was followed, namely, precipitation, calcination and washing. This strategy is in line with earlier reports suggesting that moderate substitution of Ag increases conductivity by generation of oxygen-vacancies, so long as the doping level does not exceed the point at which the structure becomes structurally unstable.

Electrochemical measurements: Determination of the electrochemical characteristics was done in a standard three electrode cell in the presence of 1 M KOH at a room temperature to isolate the intrinsic response of the $NiMoO_4$-based working electrodes and prevent the possibility of counter electrode polarisation, which is recommended best practice to assess the pseudocapacitive oxides in alkaline conditions. Pre-cleaned indium tin oxide (ITO) substrate working electrodes were produced through an aqueous slurry technique: 6 mg of active material and 1 mg of carbon black were initially mixed in deionised water under stirring and 1 mg of sodium carboxymethyl cellulose (CMC) and a little styrene butadiene rubber (SBR) were added to fine-tune viscoelasticity and adhesion. Continuous electronic percolation of the ITO substrate and isolation of the intrinsic pseudocapacitive behaviour of $NiMoO_4$ was carefully optimised by the conductive carbon content. The resulting shear-thinning slurry was the combination of which viscosity was controlled by CMC content and dispersion, which was conducive to homogeneous percolation in the carbon binder domain. The mixed product was magnitudinally stirred and ultrasonically sheared and doctor-laid onto ITO and dried at 80 ºC over 12 h to reduce migratory tendencies of the binder during drying; otherwise, binder mobility will cause interfacial resistance and reduce cohesion/adhesion. The existence of such effects is well-known with slurry-cast electrodes, the drying kinetics and temperature of which heavily affect the spatial distribution of soluble binders. The resulting films had enhanced 1.0 mg/electrode of active material and the internal conductive carbon network minimised charge-transfer resistance and facilitated the Faradaic reactions at high rates in hybrid oxide-carbon structures. A standard Ag/AgCl electrode was selected as the reference electrode and platinum foil as the counter electrode because both have a stable chemical nature and can give consistent potentials in alkaline solution conditions allowing any potential resolved analysis of the working electrode. It is important to observe that Ni-based oxides can undergo surface reconstruction when exposed to an alkaline bias to NiOOH-like phases and therefore a three-electrode set-up is crucial in deconvoluting such transformations compared to cell-level artifacts. Electrochemical measurements (cyclic voltammetry (CV), galvanostatic charge discharge (GCD) and electrochemical impedance spectroscopy (EIS)) were carried out on a CHI660E workstation. This experimental procedure is consistent with established supercapacitor fabrication protocols, where careful control of electrode formulation, adhesion and drying is essential for optimising mesostructure and charge transport within oxide-based electrodes.

RESULTS AND DISCUSSION

XRD studies: The XRD spectra of pristine $NiMoO_4$ and Ag-incorporated $NiMoO_4$ (3-7 wt.%) retain the typical reflections of monoclinic $NiMoO_4$, which has been previously reported that $NiMoO_4$ prepared *via* precipitation/hydrothermal pathways crystallizes in the monoclinic phase without forming any secondary phases to attain electrochemical activity [17] (Fig. 1a-d). Herein, the diffraction peaks of the pristine $NiMoO_4$ exhibited well-defined diffraction peaks corresponding to the $(\bar{2}11)$, $(\bar{1}21)$, $(\bar{1}12)$, $(\bar{3}01)$, (220), $(\bar{3}12)$, (040), (321) and (330) planes, which appeared at 2θ values of 21.7º, 24.0º, 25.3º, 28.2º, 28.8º, 32.8º, 41.2º, 43.2º and 43.9º, respectively. Notably, the fact that there are no other diffraction peaks that can be attributed to a metallic Ag or crystalline AgO_x means that Ag is not a long-range ordered segregated phase but is more likely to be found in a highly dispersed state and/or accommodated within the oxide (*e.g.* substitutional/interstitial incorporation, defect-associated clusters or amorphous Ag-containing domains below typical XRD detection limits). In addition, the presence and distribution of Ag in the modified samples are further supported by complementary characterisation techniques such as SEM–EDS elemental analysis and XPS measurements, which confirm the existence of Ag species in the $NiMoO_4$ system. The observed peak shifting and broadening suggest dopant-induced lattice perturbation and increased lattice microstrain, which are commonly associated with defect formation in doped transition-metal oxides [18,19]. The observed peak shifting and broadening with increasing Ag content suggest dopant-induced lattice perturbation, increased lattice microstrain and a reduction in crystallite size, which are commonly associated with defect formation in doped transition-metal oxides. Such imperfect crystallinity is usually not deleterious in the case of functional $NiMoO_4$ electrodes; it may also be a structural marker of defect development particularly oxygen-vacancy related disorder intentionally engineered to enhance the electronic conductivity and activate more Faradaic sites in $NiMoO_4$-based charge-storage materials [20,21]. Therefore, the stabilised monoclinic state and Ag-controlled peak formation that Ag primarily acts as a defect/strain modulator (and could also be a nanoscale conductivity promoter) and this offers crystallographic basis to the longstanding found enhancements in charge-transfer kinetics and utilisation of redox-active sites in electrodes of modified $NiMoO_4$.

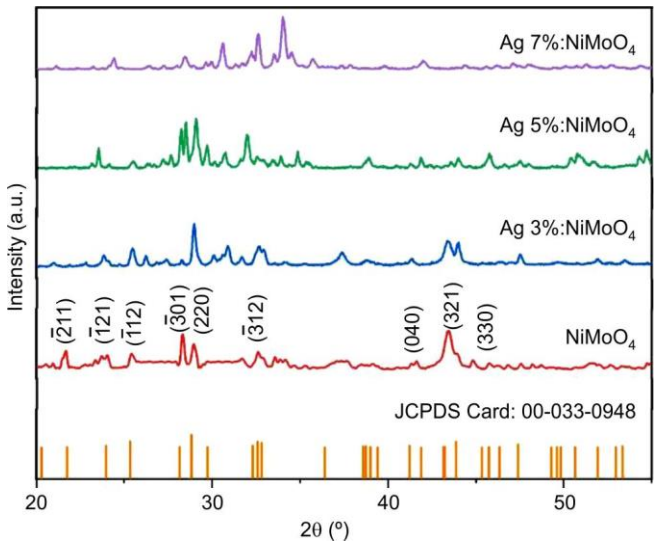

Fig. 1. XRD patterns of pristine $NiMoO_4$ and Ag-doped $NiMoO_4$ (3, 5 and 7 wt.%)

SEM studies: The use of SEM micrographs shows that Ag incorporation has a strong effect on the microstructural organisation of $NiMoO_4$ in the 3-7 wt.% doping range of the material resulting in a systematic variation in the particle dispersion, surface texture and interparticle porosity (Fig. 2a-c). $NiMoO_4$ particles at 3 wt.% Ag contain a loosely packed structure of irregular plate and rod-shaped fragments that have very large interparticle voids. Although this porosity allows easy penetration of electrolytes, the interparticle connectivity is limited implying that there are not optimal electronic transport pathways. When the Ag content is further raised to 5 wt.%, the microstructure is more refined and homogenous. The smaller particulates are evenly spread and cover the bigger flakes developing a porous network that is well-interconnected. The electrochemical characteristics of this architecture provide a favourable balance between electrochemically active surface area and efficient ion/electron transport pathways, thereby promoting rapid redox kinetics and enhanced charge transfer [22]. The $NiMoO_4$ framework at larger loading (7 wt.%) transforms into a highly textured and densely interconnected structure with an increased surface roughness and better particle-to-particle contact. Even though partial agglomeration and local densification is achieved, the architecture generated allows continuous electronic circuits and allows electrolyte-

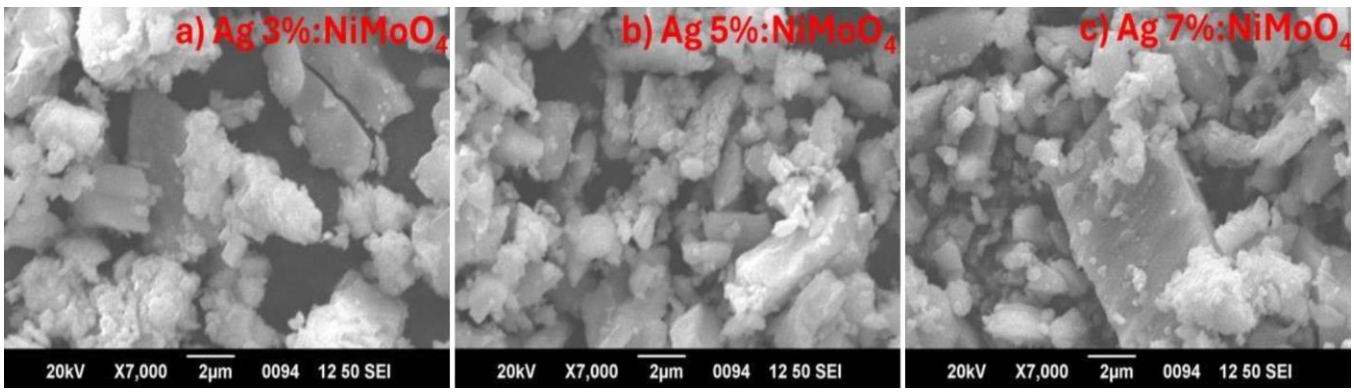

Fig. 2. SEM images of Ag-doped $NiMoO_4$ with different doping levels: (a) 3 wt.%, (b) 5 wt.% and (c) 7 wt.%

accessible porosity to prevail. The improved dispersion and reduced particle aggregation in the Ag-modified samples may contribute to enhanced electrolyte accessibility and shorter ion diffusion pathways, thereby facilitating improved electrochemical charge-storage behaviour. The particle size estimated from SEM images is approximately 50-120 nm. This synergy between enhanced electronic connectivity and surface structure with defects is in line with effective use of redox-active sites, hence the excellent performance of 7 wt.% Ag:$NiMoO_4$ electrode in electrochemical activity [22]. In general, the SEM analysis shows that moderate loading of Ag (5 wt.%) facilitates uniformity and optimal porosity whereas further loading of Ag (7 wt.%) facilitates the increase in electronic connectivity and structural integrity. This effect dominates the electrochemical response and leads to enhanced charge-storage performance despite slight microstructural densification. These findings highlight the strong interplay among morphology, electrical conductivity and defect chemistry in governing the pseudocapacitive behaviour of Ag-modified $NiMoO_4$ electrodes.

EDS studies: The spectra/mappings of the EDS confirm that Ni, Mo and O are presently in $NiMoO_4$ host and Ag is effectively added to all the doped samples with the Ag signal increasing with the doping concentration; 3 wt.% until 7 wt.%, which is in line with the fact that Ag population is doping dependent (Fig. 3a-c). Although EDS primarily provides elemental compositional information and cannot independently confirm lattice substitution, the presence of Ag signals across the examined regions indicates that Ag is well dispersed within the $NiMoO_4$ matrix rather than forming large segregated metallic particles. At the same time, the spatial distribution appears locally heterogeneous, with bright Ag-rich regions indicating that a portion of the Ag species is preferentially concentrated near particle surfaces or interparticle boundaries rather than being uniformly distributed throughout the bulk lattice. Such behaviour is commonly observed in SEM-EDS analyses when secondary components decorate or partially cover oxide microstructures [23]. Observed differences between nominal doping and EDS-derived wt.% (particularly in spot/region analysis) are likely to be taken as the sensitivity of EDS quantification to the near-surface, interaction-volume-weighted nature and its susceptibility to local composition and morphology [24]. Such Ag-enriched surface/percolation regions can be forming more efficient electronic pathways and interfacial charge-transport bridges, which can be compared to the conductivity enhancement observed when $NiMoO_4$ is combined with conductive networks or conductive interfaces [24]. However, at higher Ag loading (7 wt.%), excessive Ag enrichment may partially cover the electrochemically active surface of $NiMoO_4$ or promote local agglomeration, thereby reducing electrolyte-accessible redox sites despite improved conductive coverage. This reflects a common trade-off in defect- and interface-engineered $NiMoO_4$ systems, where enhanced conductivity can occur at the expense of active-site exposure [25].

Raman studies: Raman spectrum of pure $NiMoO_4$ shows the typical internal vibrations of the MoO_x polyhedra along with lower wavenumber lattice modes whereas Ag incorporation results in an apparent concentration dependent redshift and a gradual increase in band broadness, which indicates dopant induced lattice expansion/strain and loss of local symmetry. These changes in the $NiMoO_4$ vibrational features to lower wavenumbers have commonly been attributed to alterations in the metal oxygen vibrational environment (weakening/elongation of bonds) of $NiMoO_4$-based structures in the presence of a distorted structure and defects in the material. Their higher linewidths with Ag also suggest increased disorder and a lower phonon coherence length, which agrees with the ideas of strain-engineering that have been developed on doped $NiMoO_4$, where strain/defect chemistry of the lattice is the variable of interest in reactivity and transport. In addition, systematic variations in the Mo–O stretching region (generally dominating the high-wavenumber) are also correlated with oxygen-deficiency related perturbations of the Ni–O–Mo network; *in situ* Raman experiments of O-deficient $NiMoO_4$ systems also emphasize that defect-mediated electronic/structural reorganisation is found in the vibrational response in functional conditions [26]. Altogether, Fig. 4 confirms that Ag is principally a lattice/defect modulator as opposed to the introduction of a new crystalline phase and an intermediate level of Ag to offer the optimal compromise between defect-induced polarizability/transport enhancement and excessive disorder that can destroy structural coherence.

XPS studies: The XPS spectrum in wide scan of the 7 wt.% Ag:$NiMoO_4$ sample proves that Ni, Mo and O coexist host combined with a separate Ag signal and the C signal is produced by adventitious surface carbon as the main source of charge referencing (Fig. 5a-f). The Ni $2p_{3/2}$ and Ni $2p_{1/2}$

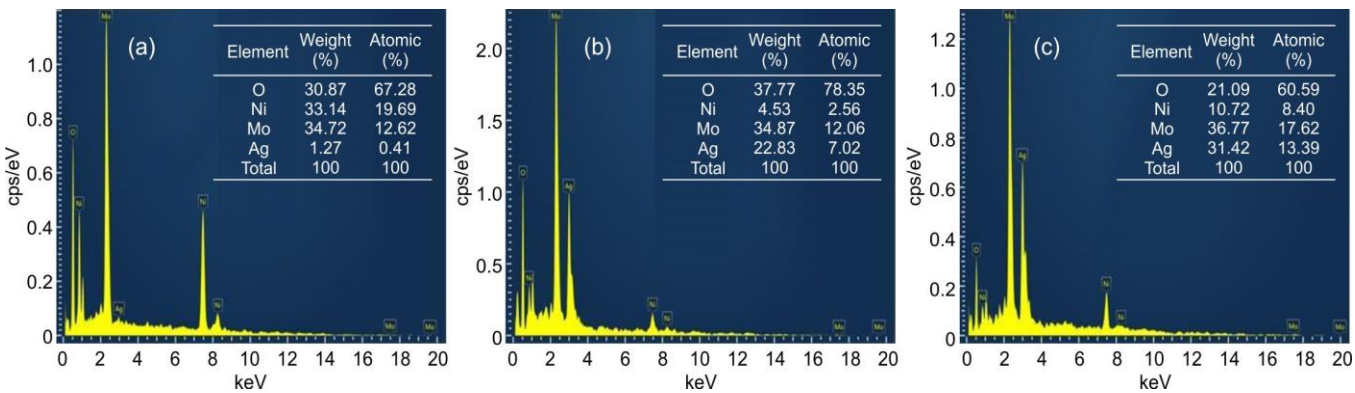

Fig. 3. EDS images of Ag-doped $NiMoO_4$ with different doping levels: (a) 3 wt.%, (b) 5 wt.% and (c) 7 wt.%

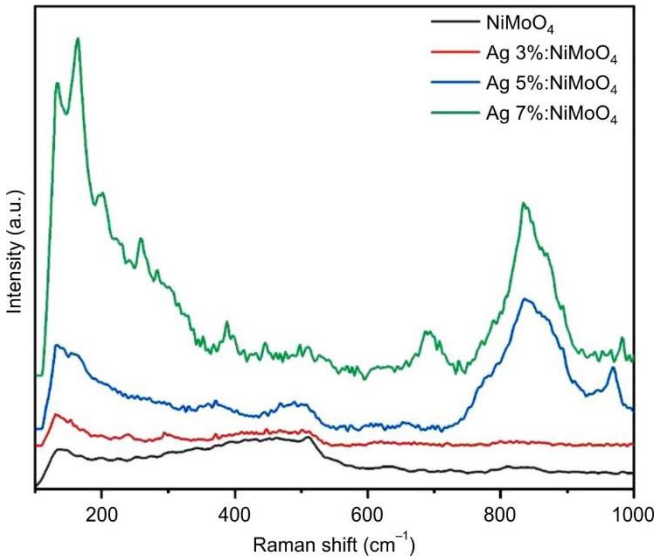

Fig. 4. Raman spectra of pristine $NiMoO_4$ and Ag-doped $NiMoO_4$ with different doping concentrations (3, 5 and 7 wt.%)

doublet with the shake-up satellites in the high-resolution Ni 2*p* region is with the Ni in oxidic environments where surface redox-active character, which is a hallmark of Faradaic charge storage and catalytic behaviour in $NiMoO_4$-based electrodes, is present binding energies at 855.36 and 872.91 eV corresponding to Ni $2p_{3/2}$ and Ni $2p_{1/2,}$ respectively [27]. The Mo 3*d* spectrum shows the Mo $3d_{5/2}$, Mo $3d_{3/2}$ two peaks at 231.77 and 234.92 eV doublet with binding energies characteristic of Mo^{6+} in molybdate structures, suggesting that the introduction of Ag does not fundamentally alter the Mo-centered molybdate lattice chemistry, is correlated with reports that show performance gains are made through surface modulation though the $NiMoO_4$ backbone is maintained [27]. The Ag $3d_{5/2}$, $3d_{3/2}$ primarily exhibits two strong bands at 367.13 eV and 373.17 eV peaks confirm successful incorporation of Ag; the shape and location of the line is typically interpreted as Ag being in a reduced state (*i.e.* Ag^0) or weakly oxidised state at the surface, which is consistent with Ag being a highly conducting component and/or in a metal-oxide junction state that supports charge transfer but is not dominant over Ag-oxide phase [28]. Oxygen deconvolution of the O 1*s* envelope normally separates a large lattice oxygen term (M–O) and a higher binding-energy term associated with surface hydroxyl bonded species and defect-related oxygen. A strengthened defect-related O 1*s* signal has often been used as a signature of oxygen-vacancy-rich surfaces in $NiMoO_4$ a feature that has been consistently reproducibly correlated with fast electronic conductivity and density of electrochemically accessible sites. These chemically absorbed/activated oxygen species are also in agreement with general XPS observations in Ni-containing oxides, where one or more oxygen condition can co-exist on particle surfaces and play a role in surface electronic condition [28]. Quantitative analysis of the XPS spectra was performed based on peak area integration after background correction. The XPS survey spectrum confirms the presence of Ni, Mo, O and Ag elements in the Ag-modified $NiMoO_4$ samples. The O 1*s* spectrum can be deconvoluted into two main components corresponding to lattice oxygen (M–O) and defect-related oxygen species associated with oxygen vacancies or surface hydroxyl

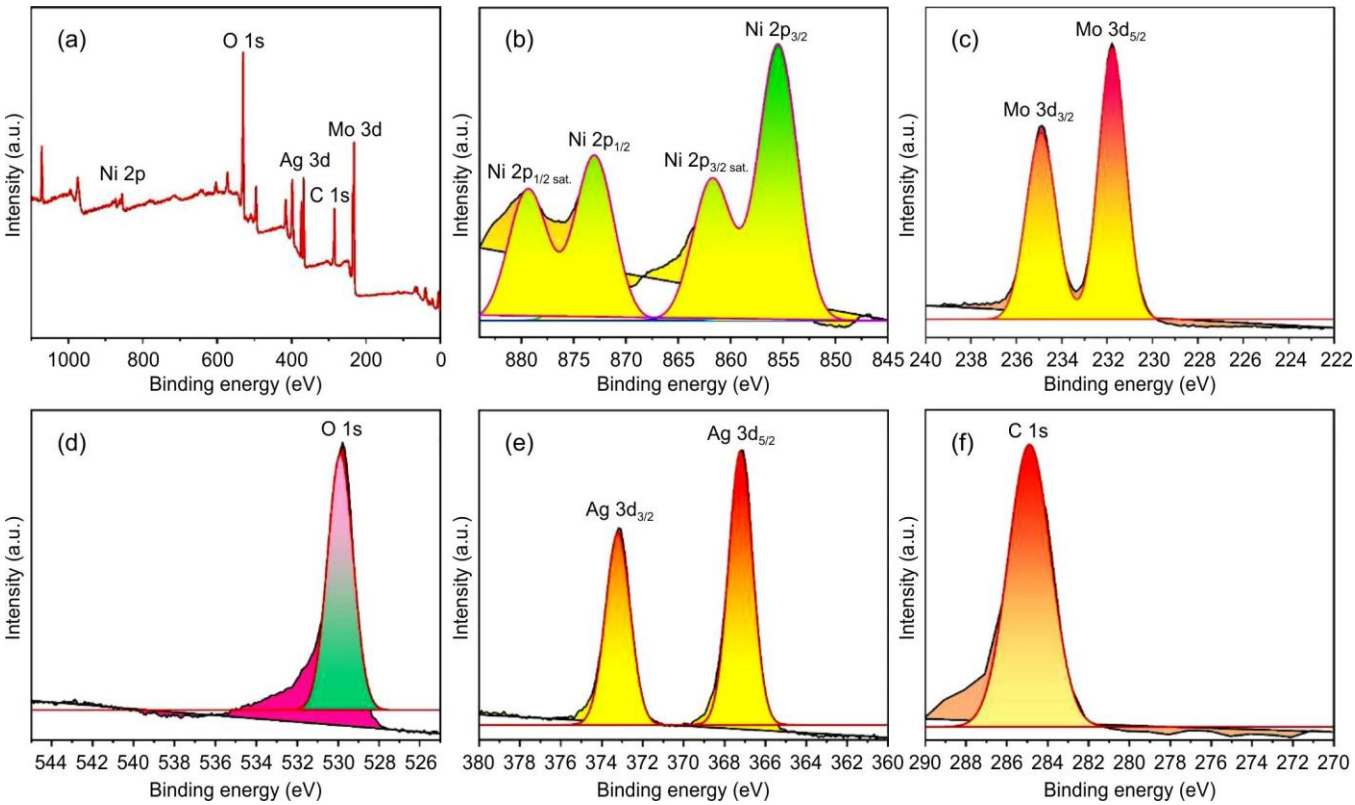

Fig. 5. XPS spectra of 7% Ag-doped $NiMoO_4$ (a) A wide range scan spectrum; (b) Ni 2*p*; (c) Mo 3*d*; (d) Ag 3*d*; (e) O 1*s*; (f) C 1*s* energy regions

groups. The relative increase in the defect-related oxygen component in Ag-modified samples suggests the formation of additional oxygen vacancy-related defects, which may contribute to improved electronic conductivity and enhanced electrochemical performance [27,28]. Fig. 5 suggests a model in which the $NiMoO_4$ host (Mo^{6+} with Ni–Mo–O framework) is held together and the addition of Ag facilitates a more conductive surface/ interface environment, as well as defect/hydroxylated oxygen species-transformations that are likely to underlie an increase in the rate of interfacial charge transfer and increasing use of Ni redox sites in the Ag-modified electrode. These results indicate that Ag not only improves electronic conductivity but also modulates defect chemistry and microstructural connectivity, thereby contributing to enhanced the electrochemical charge-storage behaviour.

Electrochemical analysis

Cyclic voltammetry (CV) studies: Cyclic voltammetry (CV) curves of pure $NiMoO_4$ and Ag-containing $NiMoO_4$ electrodes (3, 5 and 7 wt.% Ag) are not rectangular-shaped (Fig. 6), but display strong anodic and cathodic redox reactions of these electrodes, which is typical of a battery-like pseudocapacitive charge-storage mechanism that is usually dominated by reversible Faradaic reactions, which is usually the Ni^{2+}/Ni^{3+} redox couple in an alkaline electrolyte [29]. Such electrochemical properties are typical of the $NiMoO_4$-based electrode and it reflects that the charge storage is mainly in the form of the surface and near-surface redox processes. As the scan rate increases, the current responses on all the electrodes increases progressively with increasing scan rate with corresponding broadening of peaks and slight decreasing shifts of peaks to higher and lower potentials of anodic and cathodic processes, respectively. These modifications indicate polarisation effects that increase with finite charge-transfer kinetics and ion-diffusion constraints in the electroactive matrix, which is typically a common behaviour with pseudocapacitive transition-metal oxides [29]. Stable distinct redox characteristics even at increased scan rates imply a high level of electrochemical reversibility and structural integrity of the electrodes. The Ag-modified sample with the highest redox peak currents and the least potential separations between the anodic and cathodic peaks in a scan-rate range is the 5 wt.% Ag-$NiMoO_4$

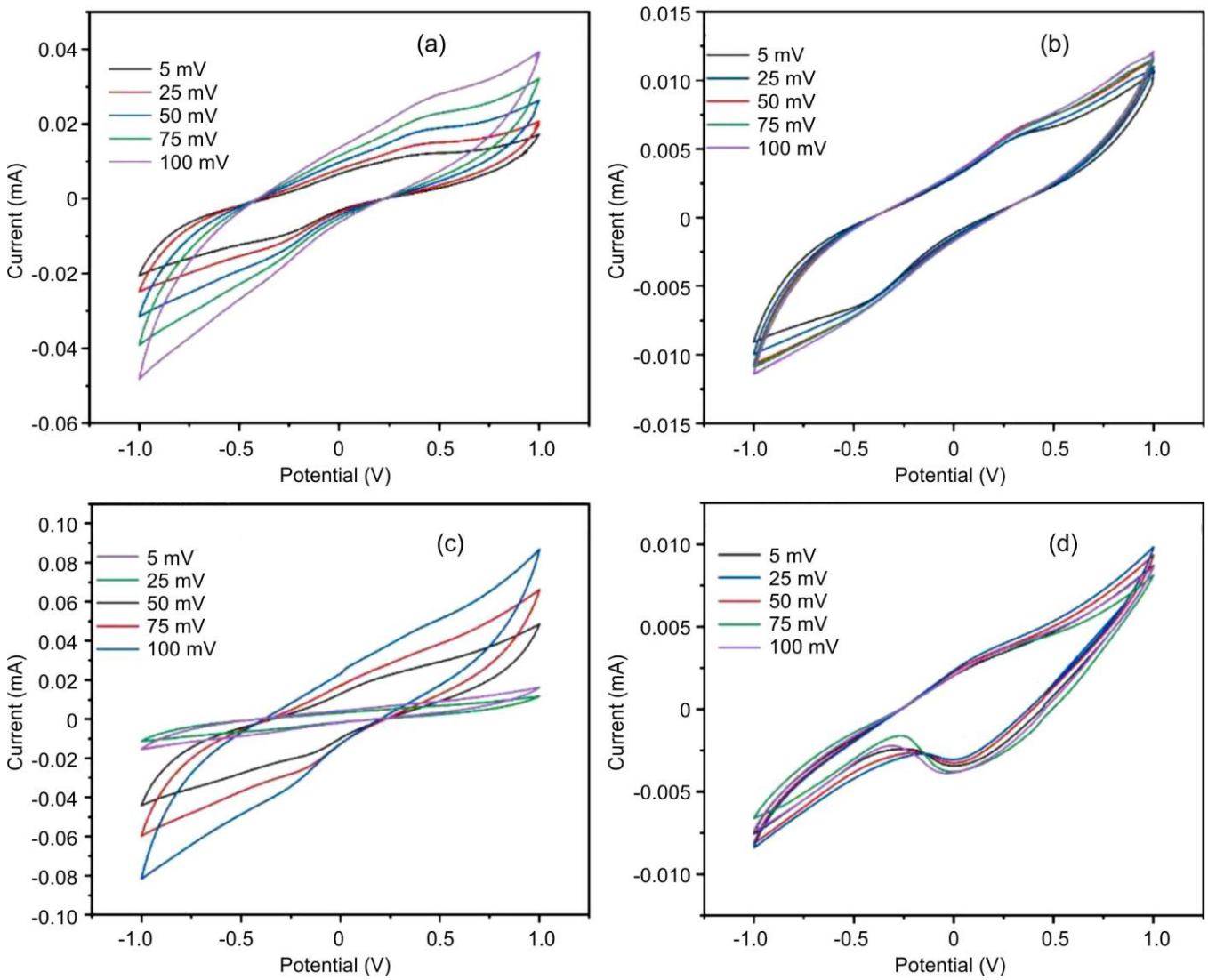

Fig. 6. CV graphs of (a) pristine $NiMoO_4$ and Ag-doped $NiMoO_4$ with different doping levels: (b) 3 wt.%, (c) 5 wt.% and (d) 7 wt.%

electrodes. This behaviour is associated with increased kinetics of charge-transfer and more efficient occupation of electrochemically accessible redox sites, which can be explained by an optimised balance between electronic conductivity, defect density and ion-transport pathways provided by moderate incorporation of Ag [30]. Conversely, clean $NiMoO_4$ shows lower peak currents and wider redox curves, which is in line with inherently reduced electronic conductivity and slower reaction rates of the material [31]. Even though the 7 wt.% Ag-$NiMoO_4$ electrode has a slightly larger separation in the peaks and slightly lower kinetic response than the 5 wt.% sample, it represents the largest CV area, meaning it has a higher total charge-storage capacity. This higher capacitance is explained by more defect density and better electronic connectivity which allow a higher fraction of redox-active sites to take part in charge storage, although ion-transport kinetics may become moderately limiting at higher Ag loading [32,33]. The 3 wt.% Ag-$NiMoO_4$ electrode is intermediately behavioural and is a good indicator of partial enhancement of conductivity and redox sites accessibility. The CV analysis reveals a clear distinction between electrochemical kinetics and total charge-storage capacity. Moderate Ag incorporation (5 wt.%) provides optimal redox kinetics and charge-transfer efficiency, whereas higher Ag loading (7 wt.%) achieves the maximum capacitance due to increased utilisation of redox-active sites. These findings demonstrate that Ag content plays a critical role in balancing electrochemical kinetics and charge storage capacity in $NiMoO_4$-based pseudocapacitive electrodes.

Following 5000 consecutive CV cycles (Fig. 7a-d) all electrodes maintain the typical Faradaic (battery-type) redox couple of $NiMoO_4$ and only slight alterations in peaked position and shape, which demonstrates that the Ni-based redox process and structural integrity of the electrodes can be repeated under polarisation conditions, which is a necessary condition of the $NiMoO_4$ electrodes, which otherwise tends to suffer gradual kinetic losses and partial loss of capacity during long-term cycling [34]. Ag incorporation significantly improves the long-term electrochemical stability of pristine $NiMoO_4$ (Fig. 7a), as evidenced by better preservation of the enclosed CV area and enhanced retention of peak current response after repeated cycling. Among the investigated electrodes, 7 wt.% $AgNiMoO_4$ exhibits the highest cycling stability. Electrode exhibits most retention (≈ 97.8%), suggesting that Ag is efficient in alleviating cycling-induced deactivation pathways

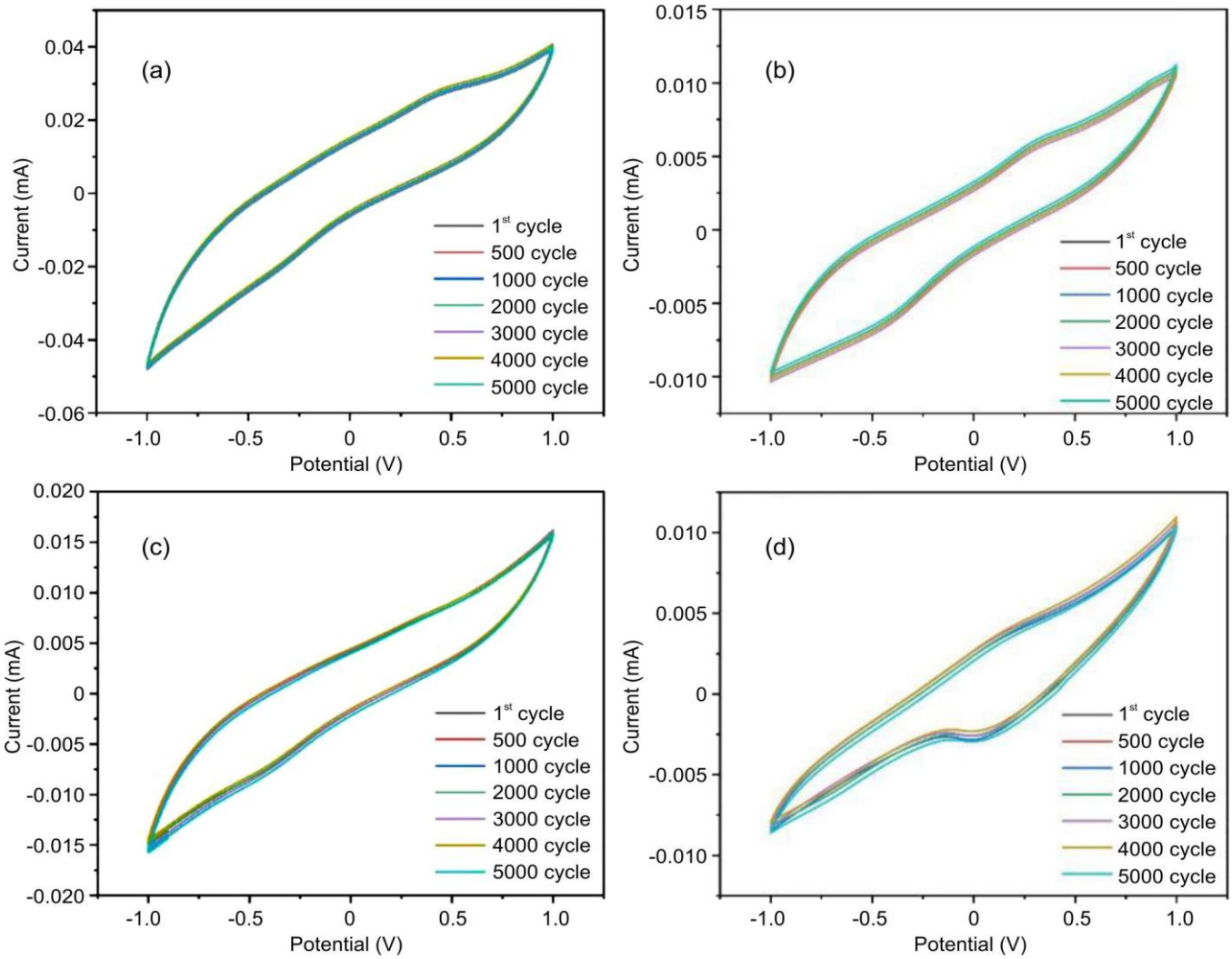

Fig. 7. 5000 Cycles of CV curve (a) pristine $NiMoO_4$ and Ag-doped $NiMoO_4$ with different doping levels: (b) 3 wt.%, (c) 5 wt.% and (d) 7 wt.%

(*e.g.* slow electron transport and loss of access to an active site). This stabilizing action is in line with the more general rule that the introduction of conductive elements and defect/ porosity engineering in $NiMoO_4$ can improve continuity of charge-transfer and retain electrochemically active redox sites throughout longer cycling. Gradual polarisation growth (increased internal resistance and interfacial barriers to charge-transfer), which accumulates in transition-metal-oxide pseudocapacitive electrodes during long cycling may explain the small anodic/cathodic shifts and slight broadening of the peak, but the relatively smaller drift in Ag-doped samples suggests more stable interfacial environment (electron/ion) of transport. Generally, Fig. 7d shows that Ag plays a synergistic role of maintenance of redox-site usage and inhibition of cycling-induced kinetic degradation with the maximum loading of Ag providing the most durable CV response when subjected to 5000-cycle operation. Table-1 indicates that the incorporation of Ag significantly increases the maximum capacitance derived by the CV of $NiMoO_4$, which rises to 342.47 F g^{-1} (pristine), 404.97 F g^{-1} (3 wt.% Ag), 592.98 F g^{-1} (5 wt.% Ag) and 642.12 F g^{-1} (7 wt.% Ag) respectively, showing progressive improvement in the electrochemical utilisation of the redox-active $NiMoO_4$ redox sites. These improvements are in line with the traditional role of forming more conductive/percolating charge pathways and expanding the electrochemical accessible interface (reducing charge-transfer losses and allowing a larger fraction of Faradaic participation), which is well-documented in case of $NiMoO_4$ when interred with conductive/transport-promoting materials and hierarchies [35]. Simultaneously, Ag has been successfully known to be an effective conductivity modifier in Ni-based battery-type electrodes to enhance capacitance achievable by enhancing the speed of interfacial electron movement and reaction kinetics. It is observed that the capacitance retention change is minor over the Ag content (99.32%→ 97.81%) and thus the capacitance enhancement due to Ag addition is attained at a relatively low cost in terms of durability and the slight reduction in capacitance retention with increasing loading is possibly due to additive side effects on interfacial/ microstructure (*e.g.* partial masking of active oxide surface or local heterogeneity) which, to a small extent, can enhance polarisation when repeated cycling with all compositions is performed. In general, the data reveal that there is a viable trade-off where, at high Ag loading, the maximum stored charge is achieved (maximum at 7 wt.%) and at very low Ag (or pristine) the retention is slightly greater, with all samples remaining extremely stable at about 98.99%.

TABLE-1
Ag DOPED $NiMoO_4$ SPECIFIC CAPACITANCE VALUES AND PERCENTAGE OF RETENTION CALCULATED BY CV

Nanocomposites (%)	Specific capacitance value (F g^{-1})	Retention (%)
$NiMoO_4$	342.47	99.32
Ag 3%:$NiMoO_4$	404.97	99.22
Ag 5%:$NiMoO_4$	592.98	98.21
Ag 7%:$NiMoO_4$	642.12	97.81

Galvanostatic charge discharge (GCD) analysis: The galvanostatic charge discharge (GCD) curves of the pure $NiMoO_4$ and Ag-doped $NiMoO_4$ (3, 5 and 7 wt.%) show distinctly non-linear trace of charge/discharge curves, without ideal triangular-shaped curves (Fig. 8), which is a good indicator of a battery-type/pseudocapacitive Faradaic storage process, as previously reported to occur in $NiMoO_4$ electrode during GCD testing, using alkaline electrolyte [36]. Compared with pristine $NiMoO_4$, Ag incorporation systematically increases the discharge time at identical current densities and reduces the initial ohmic (IR) drop. These changes indicate improved charge delivery and lower internal resistance, resulting from enhanced electronic transport and increased accessibility of redox-active sites. Such behaviour is consistent with the role of conductivity and interface engineering in improving charge-transfer kinetics in $NiMoO_4$-based electrodes [37]. The longer discharge time of the doped samples is most clearly observed at increased contents of Ag (5 and 7 wt.%), indicating that a continuous conductive network and enhanced interfacial charge transfer processes are formed when Ag loading is increased (Table-2). Similar Ag-enhanced increases in battery-type electrode behaviour are broadly ascribed to faster electron percolation and minimised interfacial impediments to OH-coupled redox reactions. The near-symmetry of charge and discharge arms in all compositions is again indicative of good reversibility and any slight polarisation escalation at the top Ag electrode can be justified by the emergence of mass-transport constraints (*e.g.* partial surface blocking/heterogeneity) associated with heavy modification even with the reduction in electronic resistance [38]. To further highlight the significance of the present work, the electrochemical performance of Ag-modified $NiMoO_4$ is compared with previously reported $NiMoO_4$-based electrodes (Table-3).

TABLE-2
Ag DOPED $NiMoO_4$ SPECIFIC CAPACITANCE VALUES CALCULATED BY GCD

Nanocomposites (%)	Specific capacitance value (F g^{-1})
$NiMoO_4$	249.12
Ag 3%:$NiMoO_4$	693.14
Ag 5%:$NiMoO_4$	888.78
Ag 7%:$NiMoO_4$	1066.12

Although the Ag-7 wt.% $NiMoO_4$ electrode exhibits a high specific capacitance of 1066.12 F g^{-1}, it should be noted that capacitance values derived from cyclic voltammetry (CV) and galvanostatic charge–discharge (GCD) measurements may differ due to the distinct calculation methods and experimental conditions associated with each technique. In CV measurements, the calculated capacitance strongly depends on the scan rate and may underestimate the full charge-storage capability because electrolyte ions cannot completely access all electroactive sites at higher scan rates. In contrast, GCD measurements performed at relatively lower current densities allow sufficient ion diffusion and more complete utilisation of Faradaic redox sites, which can lead to higher calculated capacitance values [39,40]. Therefore, the higher capacitance obtained from GCD analysis compared to CV results is consistent with the pseudocapacitive behaviour of Ag-modified $NiMoO_4$ electrodes. It should also be noted that although the

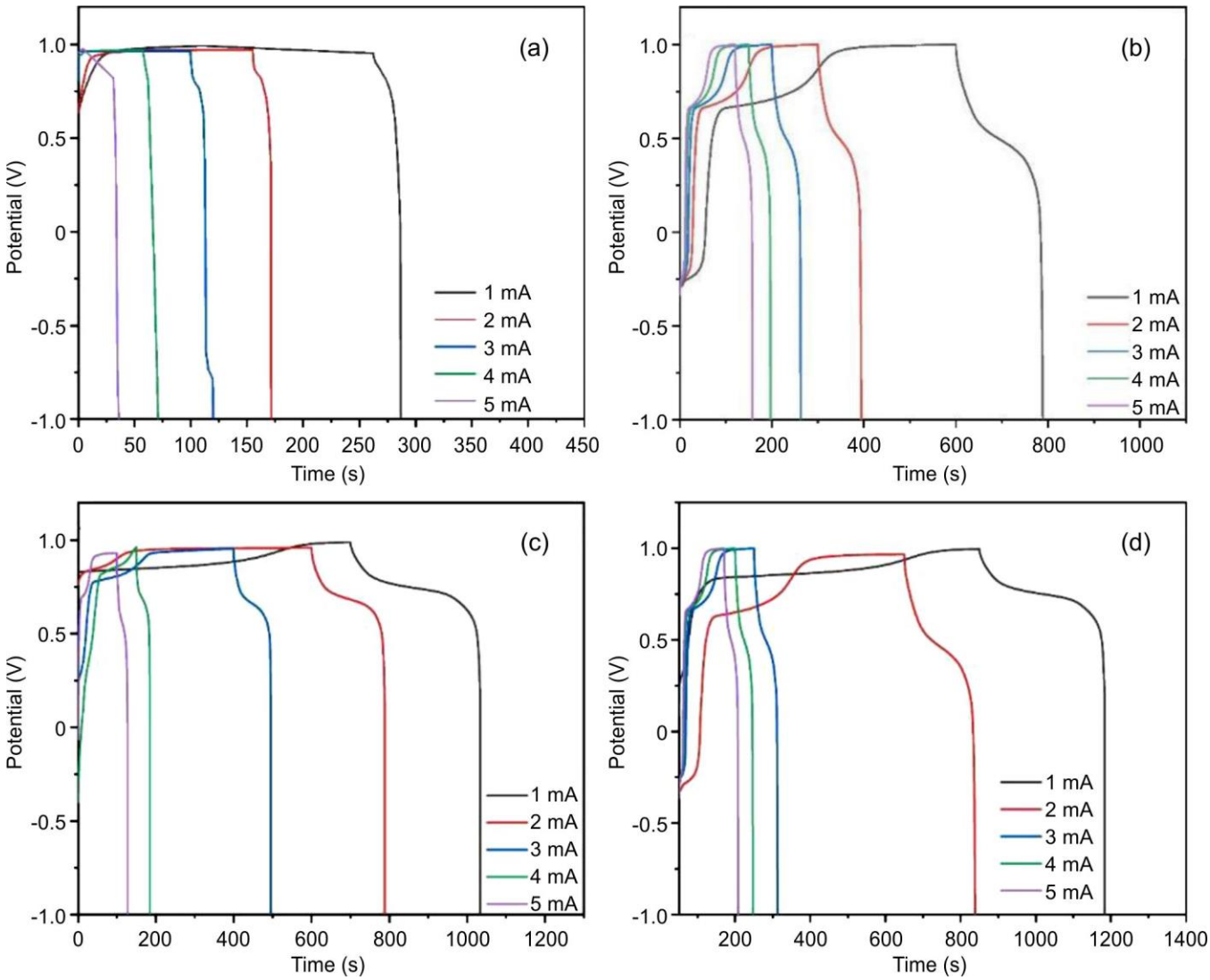

Fig. 8. GCD curves (a) pristine $NiMoO_4$ and Ag-doped $NiMoO_4$ with different doping levels: (b) 3 wt.%, (c) 5 wt.% and (d) 7 wt.%

TABLE-3
COMPARATIVE PERFORMANCE OF Ag-DOPED $NiMoO_4$ OF SYNTHESIS METHOD, ELECTRODE SUBSTRATE, SPECIFIC CAPACITANCE VALUE AND ELECTROLYTE

Material	Synthesis method	Electrode coating substrate	Specific capacitance value ($F\ g^{-1}$)	Electrolyte	Ref.
$NiMoO_4$	Microwave-combusted	Nickel foam	224.0	KOH	[39]
$NiMoO_4$	Hydrothermal method	Nickel foam	583.0	KOH	[40]
$NiMoO_4$	Hydrothermal synthesis	Nickel foam	357.6	KOH	[41]
$Mn_3O_4/NiMoO_4$@NiCo	Hydrothermal method	Carbon cloth	815.0	KOH	[42]
$NiMoO_4$@Co_3O_4	Hydrothermal method	Nickel foam	15.56	KOH	[43]
$NiMoO_4$@MnO_2	Hydrothermal method	Nickel foam	109.1	KOH	[44]
$NiMoO_4$	Impregnation method	Graphitic	541.0	H_2SO_4	[45]
$NiMoO_4$/NRGO	Hydrothermal method	Nickel foam	721.0	KOH	[46]
$NiMoO_4$-rGO	Co-precipitation method	Nickel foam	884.0	KOH	[47]
NCMO@MoS_2	Ball-milling technique	Nickel foam	571.42	KOH	[48]
Ag 7%:$NiMoO_4$	Co-precipitation method	ITO plate	1066.12	KOH	This work

electrode was deposited on an ITO substrate rather than a highly porous three-dimensional current collector such as nickel foam, the high capacitance values can still be achieved due to several factors. ITO provides sufficient electronic conductivity for thin-film electrochemical measurements, while the relatively low active material loading can lead to higher gravimetric capacitance values. In addition, Ag incorporation improves the electronic conductivity and promotes faster Faradaic redox reactions within the $NiMoO_4$ framework. The combined effects of improved conductivity, defect-induced active sites and effi-

cient ion transport contribute to the enhanced electrochemical performance observed in the Ag-modified $NiMoO_4$ electrodes [41]. Moreover, interfacial effects that are generated by Ag might enable a faster Faradaic kinetics in the alkaline media because it reduces the electronic/ionic transport barrier, thus increasing discharge time and increasing the calculated capacitance in the GCD condition. In general, the tendency shows that a gradual raise in the Ag content enhances continuously the use of charge-storage in $NiMoO_4$ in the interval. It is important to note that the electrochemical behaviour varies with Ag concentration [41]. The sample containing 5 wt.% Ag exhibits improved electrochemical kinetics due to its relatively uniform microstructure and balanced porosity, which facilitate efficient ion diffusion and charge-transfer processes. In contrast, the 7 wt.% Ag-incorporated sample exhibits the highest specific capacitance, which can be attributed to enhanced electronic conductivity and the increased availability of electrochemically active sites within the $NiMoO_4$ framework [41]. Although higher Ag loading may induce slight structural densification or localised agglomeration that can partially influence ion transport kinetics, the increased conductive pathways and greater availability of redox-active sites contribute to enhanced charge-storage capacity. This behaviour reflects a balance between ion diffusion kinetics and electronic conductivity in determining the electrochemical performance of Ag-modified $NiMoO_4$ electrodes.

Electrochemical impedance spectroscopy (EIS) studies: The EIS was used to further clarify the manner of charge-transfer resistance and ion-transport of pristine and Ag-doped $NiMoO_4$ electrodes. The characteristic curve of the battery-type pseudocapacitive electrodes as shown by the Nyquist plots (Fig. 9) include the high frequency intercept (representing resistance to solution R_s) of the curve, a depressed semicircle in the high-to-medium frequency range (representing charge-transfer resistance R_{ct}) and an inclined line in the low-frequency range (representing ion diffusion and capacitive response R_w). All the Ag-incorporated electrodes have a smaller semicircle diameter than pristine $NiMoO_4$, showing a strong reduction in charge-transfer resistance with the addition of Ag. This decrease in R_{ct} supports the fact that Ag incorporation is effective to improve the electronic conductivity and faster interfacial Faradaic reactions at the electrode electrolyte interface, which aligns with the increased redox kinetics in CV and GCD data [49,50]. The 5 wt.% Ag-$NiMoO_4$ electrode has the smallest semicircle in the doped samples, indicating the most effective process of charge-transfer and best interfacial electron-paths. The slope of the Ag-doped electrodes is steeper than that of pristine $NiMoO_4$ in the low-frequency region, which is an indication of enhanced capacitive behaviour and increased ion diffusion in the porous electrode structure. However, upon further increasing the Ag loading to 7 wt.%, a noticeable deviation from the ideal vertical line is observed, indicating the onset of diffusion limitations. This behaviour may arise from partial pore blockage or increased microstructural heterogeneity at higher Ag loading, resulting in more complex ion diffusion pathways despite improved electronic conductivity [51, 52]. The EIS results indicate that the moderate Ag incorporation effectively reduces interfacial resistance and enhances ion/electron transport, whereas excessive loading introduces

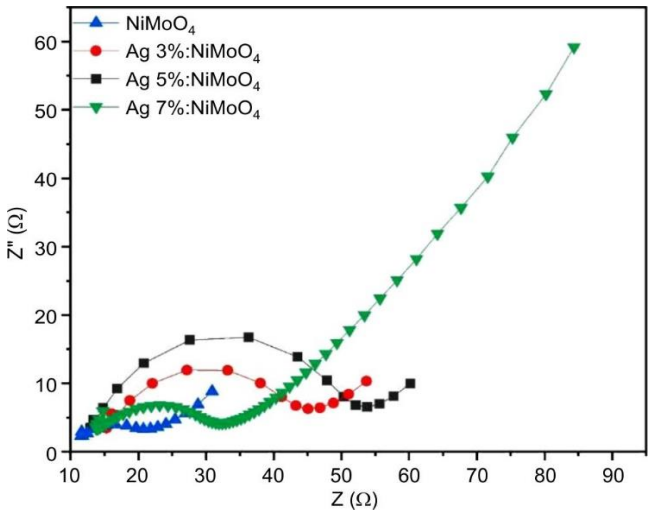

Fig. 9. EIS spectra of pristine $NiMoO_4$ and Ag-doped $NiMoO_4$ (3%, 5%, 7%)

slight diffusion limitations. These observations are consistent with the CV and GCD results, confirming that Ag incorporation improves both electronic conductivity and interfacial charge transport characteristics in $NiMoO_4$-based pseudocapacitive electrodes.

Conclusion

This work demonstrates that the controlled silver (Ag) incorporation effectively modulates structural defects, electronic conductivity and ion-transport behaviour in $NiMoO_4$ nanostructures, leading to enhanced pseudocapacitive performance. XRD analysis (established the presence of phase-pure monoclinic $NiMoO_4$ regardless of the compositions) and no secondary phases associated with Ag were identified, which shows successful insertion of Ag into the host structure. Microstructural observation indicated that Ag addition altered markedly the particle dispersion and porosity that facilitated better access to electrolytes and charge transport. Raman and XPS analysis revealed that the insertion of Ag caused a lattice distortion and the appearance of oxygen vacancy rich defect states that contribute significantly to the increase of the electronic conductivity and the introduction of the redox-active sites. Electrochemical analysis indicated that Ag-modified $NiMoO_4$ electrodes would demonstrate significantly enhanced pseudocapacitative behaviour relative to pure $NiMoO_4$. Of the compositions examined, the Ag-7 wt.% $NiMoO_4$ electrode presented the highest specific capacitance values of 642.12 F g^{-1} during cyclic voltammetry and 1066.12 F g^{-1} during galvanostatic charge discharge of 97.81% after 5000 cycles. This improvement in performance is ascribed to synergistic interaction of Ag-induced enhancement of electronic conductivity, defect-mediated charge transport and optimal ion dynamics of ion diffusion within $NiMoO_4$. Although there is a trade-off between moderate incorporation of Ag and charge transfer kinetics, further increase in Ag loading enhances redox site exploitation, indicating a balance between kinetic efficiency and overall charge storage. This study demonstrates that Ag incorporation is a viable defect and charge-transport engineering approach to $NiMoO_4$-based electrodes and the design of high-performance pseudo-capacitive materials for next-generation supercapacitor applications.

ACKNOWLEDGEMENTS

The authors sincerely acknowledge the financial and infra-structural support provided by Kongunadu Arts and Science College, Coimbatore, which made this research work possible.

CONFLICT OF INTEREST

The authors declare that there is no conflict of interests regarding the publication of this article.

DECLARATION OF AI-ASSISTED TECHNOLOGIES

During the preparation of this manuscript, the authors used an AI-assisted tool(s) to improve the language. The authors reviewed and edited the content and take full responsibility for the published work.

REFERENCES

1. V. Kannan, H.J. Kim, H.C. Park and H.S. Kim, *Nanomaterials*, **8**, 563 (2018); https://doi.org/10.3390/nano8080563
2. J.Y. Dong, J.C. Xu, K.N. Hui, Y. Yang, S.C. Su, L. Li, X.T. Zhang, K.W. Ng, S.P. Wang and Z.K. Tang, *Nanomaterials*, **9**, 1033 (2019); https://doi.org/10.3390/nano9071033
3. Z. Wang, G. Wei, K. Du, X. Zhao, M. Liu, S. Wang, Y. Zhou, C. An and J. Zhang, *ACS Sustain. Chem. Eng.*, **5**, 5964 (2017); https://doi.org/10.1021/acssuschemeng.7b00758
4. S. Arshadi Rastabi, R. Sarraf Mamoory, N. Blomquist, M. Phadatare and H. Olin, *Batteries*, **6**, 5 (2020); https://doi.org/10.3390/batteries6010005
5. K. Thiagarajan, T. Bavani, P. Arunachalam, S.J. Lee, J. Theerthagiri, J. Madhavan, B.G. Pollet and M.Y. Choi, *Nanomaterials*, **10**, 392 (2020); https://doi.org/10.3390/nano10020392
6. P. Sivakumar, C.J. Raj, J. Park and H. Jung, *Int. J. Energy Res.*, **45**, 21516 (2021); https://doi.org/10.1002/er.7156
7. Z.H. Huang, H. Li, W.H. Li, G. Henkelman, B. Jia and T. Ma, *Small*, **16**, 2004709 (2020); https://doi.org/10.1002/smll.202004709
8. P. Wang, X. Ding, R. Zhe, T. Zhu, C. Qing, Y. Liu and H.E. Wang, *Nanomaterials*, **12**, 1094 (2022); https://doi.org/10.3390/nano12071094
9. Q. Sun, Z. Guo, T. Shu, Y. Li, K. Li, Y. Zhang, L. Li, J. Ning and K. X. Yao, *ACS Appl. Mater. Interfaces*, **16**, 12781 (2024); https://doi.org/10.1021/acsami.3c18248
10. A. Jeevarathinam, A. Annamalai, S. Elumalai, S. Sangaraju and F.M. Hassan, *J. Energy Storage*, **163**, 121612 (2026); https://doi.org/10.1016/j.est.2026.121612
11. C. Chen, D. Yan, X. Luo, W. Gao, G. Huang, Z. Han, Y. Zeng and Z. Zhu, *ACS Appl. Mater. Interfaces*, **10**, 4662 (2018); https://doi.org/10.1021/acsami.7b16271
12. C.J. Raj, R. Manikandan, K.H. Yu, G. Nagaraju, M.S. Park, D.W. Kim, S.Y. Park and B.C. Kim, *Inorg. Chem. Front.*, **7**, 369 (2020); https://doi.org/10.1039/C9QI01085H
13. Z. Zeng, P. Sun, J. Zhu and X. Zhu, *RSC Adv.*, **5**, 17550 (2015); https://doi.org/10.1039/C4RA16646A
14. S. Jana, S. Pande, A.K. Sinha, S. Sarkar, M. Pradhan, M. Basu, S. Saha and T. Pal, *J. Phys. Chem. C*, **113**, 1386 (2009); https://doi.org/10.1021/jp809561p
15. Q.T. Nguyen, U.T. Nakate, B.G. Ghule, S. Park, J. Choi, J.H. Park, J.H. Jang, D.W. Kim and S. Park, *ACS Appl. Mater. Interfaces*, **17**, 12307 (2025); https://doi.org/10.1021/acsami.4c22156
16. C. Martínez-Morales, A. Romero-Serrano, J. López-Rodríguez and P. Arellanes-Lozada, *Materials*, **18**, 3869 (2025); https://doi.org/10.3390/ma18163869
17. J. Xu and H. Guo, *Chem. Lett.*, **51**, 807 (2022); https://doi.org/10.1246/cl.220225
18. J. Li, S. Liu, X. Liu, X. Peng, Y. Cao, L. Liu and J. Tong, *J. Mater. Chem. A*, **14**, 6364 (2026); https://doi.org/10.1039/D5TA08846A
19. H. Li, X. Gao, T. Wang, Z. Shi, J. Bai, Z. Wang and X. Wang, *Fuel*, **406**, 137223 (2026); https://doi.org/10.1016/j.fuel.2025.137223
20. F.K. Kerdabadi, P. Kameli, M.M. Momeni, T. Sarkar and B. Aslibeiki, *J. Mater. Chem. A*, **14**, 5751 (2026); https://doi.org/10.1039/D5TA07465G
21. A.N. Babu, K.P. Shwetha and C.G. Renuka, *J. Energy Storage*, **149**, 120238 (2026); https://doi.org/10.1016/j.est.2025.120238
22. M. Beemarao, P. Kanagambal, K. Ravichandran, P. Rajeswaran, I.M. Ashraf, U. Chalapathi and S.H. Park, *Inorg. Chem. Commun.*, **153**, 110853 (2023); https://doi.org/10.1016/j.inoche.2023.110853
23. M. Yao, Z. Yuan, J. Li, F. Liu and S. Geng, *J. Energy Storage*, **116**, 116082 (2025); https://doi.org/10.1016/j.est.2025.116082
24. D.S. Sawant, S.V. Gaikwad, A.V. Fulari, M. Govindasamy, S.B. Kulkarni, D.P. Dubal and G.M. Lohar, *Small*, **21**, 2500080 (2025); https://doi.org/10.1002/smll.202500080
25. H. Yin, X. Xing, W. Zhang, J. Li, W. Xiong and H. Li, *Dalton Trans.*, **52**, 16670 (2023); https://doi.org/10.1039/D3DT03018K
26. R.N. Dürr, P. Maltoni, H. Tian, B. Jousselme, L. Hammarström and T. Edvinsson, *ACS Nano*, **15**, 20693 (2021); https://doi.org/10.1021/acsnano.1c10145
27. F. Nti, D.A. Anang and J.I. Han, *J. Alloys Compd.*, **742**, 342 (2018); https://doi.org/10.1016/j.jallcom.2018.01.289
28. D. Essam, A.M. Ahmed, A.A. Abdel-Khaliek, M. Shaban and M. Rabia, *Sci. Rep.*, **15**, 2698 (2025); https://doi.org/10.1038/s41598-024-84848-5
29. Y. Zhidong, H. Linfeng, Y. Ruoxuan, W. Wenbin, C. Tao and J. Qi, *J. Energy Storage*, **149**, 120441 (2026); https://doi.org/10.1016/j.est.2026.120441
30. Y. Wang, Y. Cui, Y. Song and C. Zhou, *Nanomaterials*, **14**, 1798 (2024); https://doi.org/10.3390/nano14221798
31. Y. Li, J. Jian, Y. Fan, H. Wang, L. Yu, G. Cheng, J. Zhou and M. Sun, *RSC Adv.*, **6**, 69627 (2016); https://doi.org/10.1039/C6RA13955H
32. J.A.A. Mehrez, K.A. Owusu, Q. Chen, L. Li, K. Hamwi, W. Luo and L. Mai, *Inorg. Chem. Front.*, **6**, 857 (2019); https://doi.org/10.1039/C8QI01420E
33. N. Liu, R. Wu, Y. Liu, P. Deng, Y. Li, Y. Du, Y. Cheng, Z. Zhuang, Z. Kang and H. Li, *Inorg. Chem.*, **62**, 11990 (2023); https://doi.org/10.1021/acs.inorgchem.3c01467
34. F. Wang, K. Ma, W. Tian, J. Dong, H. Han, H. Wang, K. Deng, H. Yue, Y.X. Zhang, W. Jiang and J. Ji, *J. Mater. Chem. A*, **7**, 19589 (2019); https://doi.org/10.1039/C9TA04568F
35. S. Vijipriya, M. Anujency, P. N. Pratheeb, R. Bakkiyaraj and M.M. Ibrahim, *J. Indian Chem. Soc.*, **103**, 102546 (2026); https://doi.org/10.1016/j.jics.2026.102546
36. S.A. Patil, P.B. Jagdale, A. Iqbal, S. Reza, M. Jinagi, P. Rajput, A. Sfeir, S. Royer, R. Thapa, A.K. Samal and M. Saxena, *J. Mater. Chem. A*, **13**, 15782 (2025); https://doi.org/10.1039/D5TA02450A
37. Y. Chang, L. Kong, D. Xu, X. Lu, S. Wang, Y. Li, J. Bao, Y. Wang and Y. Liu, *Angew. Chem. Int. Ed.*, **64**, e202414234 (2025); https://doi.org/10.1002/anie.202414234
38. H.M. Arbi, A.A. Yadav, Y. Anil Kumar, M. Moniruzzaman, S. Alzahmi and I.M. Obaidat, *Nanomaterials*, **12**, 3982 (2022); https://doi.org/10.3390/nano12223982
39. S. Sakthivel, S. Shobika, A. Dinesh, K. Yogalakshmi, R. Suriyaprakash, B. Kabilan, P. Sathyajith, S. Elumalai, L. Gnanasekaran, M. Ayyar and M. Santhamoorthy, *Results Chem.*, **13**, 101956 (2025); https://doi.org/10.1016/j.rechem.2024.101956
40. R. Yuvaraja, S. Sarathkumar, V. Gowsalya, S. Veeralakshmi, S.P.A. Juliet, S. Kalaiselvam, G.H. Gunasekar and S. Nehru, *Energy Adv.*, **4**, 94 (2024); https://doi.org/10.1039/D4YA00438H

41. H.R. Lee, M.S. Akhtar, A. Umar, A.A. Ibrahim, S. Baskoutas and O.B. Yang, *Chem. Phys. Impact*, **8**, 100406 (2024); https://doi.org/10.1016/j.chphi.2023.100406
42. R. Liang, S. Liu, J. Lin, J. Dai, J. Peng, P. Huang, J. Chen and P. Xiao, *RSC Adv.*, **13**, 33463 (2023); https://doi.org/10.1039/D3RA06937K
43. M. Wang, J. Zhang, X. Yi, B. Liu, X. Zhao and X. Liu, *Beilstein J. Nanotechnol.*, **11**, 240 (2020); https://doi.org/10.3762/bjnano.11.18
44. A.A. Mohammed, J.K. Das, A. Hota and B.C. Tripathy, *Diamond Relat. Mater.*, **144**, 110940 (2024); https://doi.org/10.1016/j.diamond.2024.110940
45. E. Hamdi, A. Abdelwahab, A.A. Farghali, W.M.E. Rouby and F. Carrasco-Marín, *Materials*, **16**, 1264 (2023); https://doi.org/10.3390/ma16031264
46. R. Shejini, K. Mohanraj, J. Henry and G. Sivakumar, *ChemistrySelect*, **9**, e202403167 (2024); https://doi.org/10.1002/slct.202403167
47. S. Arshadi-Rastabi, R. Sarraf-Mamoory, G. Razaz, N. Blomquist, J. Örtegren and H. Olin, *J. Compos. Sci.*, **7**, 217 (2023); https://doi.org/10.3390/jcs7060217
48. K. Karami, E. Z. Jazi, N. Jamshidian and A. Allafchian, *RSC Adv.*, **15**, 16229 (2025); https://doi.org/10.1039/D5RA01168J
49. K. Panchal, K. Bhakar, K.S. Sharma, D. Kumar and S. Prasad, *Appl. Spectrosc. Rev.*, **60**, 30 (2025); https://doi.org/10.1080/05704928.2024.2361082
50. S. Das, A. Banerjee, U. Nandi and A. Ghosh, *J. Appl. Phys.*, **138**, 125002 (2025); https://doi.org/10.1063/5.0275205
51. A.K. Yedluri, T. Anitha and H.J. Kim, *Energies*, **12**, 1143 (2019); https://doi.org/10.3390/en12061143
52. Z. Sun, X. Chang, S. Qiu, S. Li and M. Zhang, *J. Alloys Compd.*, **1010**, 177580 (2025); https://doi.org/10.1016/j.jallcom.2024.177580